

1 **Spatial considerations in the transport of pollutants to indoor**  
2 **surfaces**

3

4 Glenn Morrison

5 *Department of Civil, Architectural and Environmental Engineering*

6 *University of Missouri-Rolla, 221 Butler-Carlton Hall, Rolla, MO 65409-0030*

7

8 **Abstract**

9

10 Spatial distributions in surface flux and concentrations complicate the  
11 measurement of surface mass-transfer coefficients can bias the resulting estimates of  
12 indoor exposure. To better understand these phenomena, we quantify the spatial  
13 distribution of ozone flux and mass-transfer coefficients to indoor surfaces in several  
14 field locations using NaNO<sub>2</sub> coated filters. The 8-hour average transport-limited  
15 deposition velocity for ozone,  $\bar{v}_{t,ozone}$ , ranged from 0.06 cm s<sup>-1</sup> on a wall to 0.78 cm s<sup>-1</sup>  
16 near an operating ventilation supply vent in an apartment. A narrower distribution and a  
17 lower spatial average was observed with the recirculation system off. Qualitatively, we  
18 observed 1) a tighter distribution of flux for filters placed near one-another, 2) higher  
19 values near sources of air movement such as supply vents and computers, 3) consistent  
20 results in a single location over 5 days. Measurements obtained with devices such as  
21 coated filters will exceed the “true” value of  $\bar{v}_{t,ozone}$  by a factor dependent on the size of  
22 the device, size of the room and the flow conditions within the room. Based on a

23 preliminary understanding of phenomena that influence these measurements, a  
24 combination of techniques should be used simultaneously for correction of measurement  
25 bias: time-averaged measurements, using two different sizes of devices such as coated  
26 filters, and a continuous measurement, such as evaporation of a hydrocarbon from a  
27 microbalance.

28

29 *Keywords:* mass-transfer, pollutant transport, pollutant deposition, indoor air, spatial  
30 measurement

31

## 32 **1. Introduction**

33 The transport-limited deposition velocity,  $v_t$ , is a mass-transfer coefficient that can  
34 be used directly in the analysis of pollutant flux to indoor surfaces. Flux is defined as the  
35 product of  $v_t$ , and the concentration gradient across a boundary layer that has developed  
36 over a surface. Mathematically, the local, instantaneous flux,  $J(s,t)$ , to or from a surface is  
37 given by,

$$38 \quad J(s,t) = v_t(s,t)[C_b(s,t) - C_s(s,t)] \quad (1)$$

39 where  $s$  denotes surface location or coordinates,  $t$  is time,  $C_b(s,t)$  is the concentration at  
40 the outer edge of the concentration boundary layer that has developed over a reactive  
41 surface, and  $C_s(s,t)$  is the near-surface gas concentration of the pollutant. As the flux to a  
42 surface increases, indoor concentrations decrease and vice versa. In understanding indoor  
43 systems, Eq (1) can sometimes be simplified because the magnitude of  $C_s(s,t)$  depends on  
44 dynamics taking place at the surface. For example, nitric acid deposition to an indoor  
45 surface is nearly completely irreversible, and as a result  $C_s(s,t)$  is effectively zero. In

46 contrast, for emission from a solvent spill,  $C_s(s,t)$  is the saturation concentration of the  
47 solvent.

48 In a mass-conservation model of indoor air concentrations, the area-integrated  
49 flux is the total instantaneous mass rate of change in a room due to surface  
50 interactions. Therefore, it is desirable to quantify the underlying parameters, such as  
51  $v_t(s,t)$ , that control fluxes. The term  $v_t(s,t)$  is independent of concentrations for dilute  
52 systems. Instead  $v_t(s,t)$  depends on the flow conditions near the surface and the gaseous  
53 pollutant diffusivity. Thus  $v_t(s,t)$  can be determined from location specific measurement  
54 (Morrison et al., 2003) or model calculations of flow conditions (Nazaroff and Cass,  
55 1987). However, (Nazaroff et al., 1993) cautioned that deposition rates are strongly  
56 dependent on flow conditions which will vary greatly among building types and  
57 ventilation and that using average deposition velocities for a room or building may be  
58 inappropriate since the local values may vary considerably. Thus, to improve the  
59 usefulness of the concept of deposition velocity for indoor air quality modeling and  
60 exposure assessment, we require a better understanding of the magnitude and variability  
61 of air/surface pollutant transport.

62 This research is directed to measuring the spatial distribution of ozone surface  
63 flux in several field settings. We combine these results with a theoretical consideration of  
64 bias resulting from using measurement devices which necessarily have smaller  
65 dimensions than the room dimensions to arrive at the spatial distribution of transport-  
66 limited deposition velocities. The distribution, in turn, allows us to qualitatively evaluate  
67 building characteristics that influence  $v_t$ . We estimate how spatial distribution of transport

68 influences uncertainty in models used to predict indoor concentrations. In addition, we  
69 make procedural recommendations for future mass-transport measurements in buildings.

70 *1.1 Theory: spatial variability in mass transport*

71 To demonstrate the importance of measuring the spatial distribution of transport  
72 phenomena, we first consider the infiltration of a surface reactive pollutant into a  
73 building, where concentrations and transport conditions are not uniformly distributed  
74 throughout a room. The steady-state, volume-averaged core concentration,  $\bar{C}_b$ , is here  
75 derived by balancing the mass rates of sources (infiltration) and sinks (exfiltration and  
76 surface flux):

77 
$$\bar{C}_b = C_o - \frac{1}{Q} \int_s v_t(s) [C_b(s) - C_s(s)] ds \quad (2)$$

78  
79 where  $C_o$  is the outdoor concentration,  $Q$  is volumetric infiltration rate and the integration  
80 takes place over a surface,  $s$ . If each of these parameters ( $v_t$ ,  $C_b$ ,  $C_s$ ) is spatially  
81 dependent, then the use of an area-averaged value of  $\hat{v}_t$  for modeling is not appropriate  
82 because,  $v_t$ , cannot be separated from the product within the integral. Only if  $(C_b - C_s)$  is  
83 independent of  $s$  or nearly constant in  $s$ , will it be possible to isolate area-average value  
84 of the transport-limited deposition velocity,  $\hat{v}_t$ :

85 
$$\bar{C}_b = C_o - \frac{(C_b - C_s)}{Q} \int_s v_t(s) ds = C_o - \frac{(C_b - C_s) \hat{v}_t A}{Q} \quad (3)$$

86 where  $A$  is the total surface area of the room. Only for this unique case is it accurate to  
87 report or use  $\hat{v}_t$ .

88 To estimate error introduced by this type of method, spatial distributions in  
89 concentrations and transport would be necessary, but are not readily available. The  
90 spatial-distribution measurements to be reported here provide some guidance in  
91 estimating uncertainties in measuring and using  $\hat{v}_i$ .

### 92 1.2. Spatial scales and measurement of $v_i$

93 Care must be taken when interpreting results from spatial-distribution  
94 measurements because the size of the collecting/emitting surface can influence the  
95 outcome. The stagnant-film theory model of mass transfer can be used to demonstrate  
96 this size dependent effect. Due to surface emission or deposition flux, a concentration  
97 gradient and boundary layer will develop over the measurement surface, but not  
98 necessarily over the surrounding walls. The flux in this case is equal to the product of a  
99 concentration gradient and a mass-transfer coefficient, itself equal to the diffusion  
100 coefficient,  $D$ , divided by the thickness of the stagnant film,  $\delta$ . All else being equal, as  
101 the film thickness increases the flux and the mass-transfer coefficient decrease. Non-  
102 stagnant concentration boundary layers also exhibit this behavior: the thicker the  
103 concentration boundary layer over a surface, the lower the flux and the lower the  
104 resulting mass-transfer coefficient.

105 This issue of device dimensions is addressed by considering the concentration  
106 boundary layer that has developed over a device used to measure the mass-transfer  
107 coefficient. See Fig. 1a and 1b for a two-dimensional representation of a case in which  
108 the pollutant, e.g. ozone, is consumed readily by the measuring surface but not with the  
109 surrounding walls. For example, deposition of ozone to a disk coated with a reactive  
110 media (see Methods section) is used to determine the time-averaged local mass-transfer

111 coefficient on a wall. A concentration boundary layer will develop over the disk with  
112 varying thickness depending on the fluid-mechanical nature and direction of flow as well  
113 as the distance from the edge of the disk. The value of  $v_t$  derived from disk 1 is  
114 proportional to the thickness of the boundary layer,  $\delta_1$ . If the researcher uses a larger disk,  
115 Fig 1b, the mean thickness of the concentration boundary layer will be greater,  $\delta_2$ . Given  
116 the same time interval for evaporation, the time-integrated flux will be larger for disk 1  
117 than for disk 2 and  $v_t$  derived from disk 1 will be larger than that derived from disk 2.

118         Preferably, the size of the device should not matter. This will be the case for  
119 measurements of a pollutant that tends to be consumed by all surfaces, such as acid gases,  
120 where the appropriate boundary layer for measurement should look something like Fig  
121 1c; in this figure, the concentration boundary layer develops over a wall and corner and  
122 no sensing surface is present. For this case, a continuous concentration boundary layer  
123 develops over all indoor surfaces whether a collecting surface is present or not. Since  $\delta_3 >$   
124  $\delta_2 > \delta_1$ , a measurement as shown in Fig 1a and 1b always over-predicts  $v_t$ . Unlike the  
125 ozone example, placing a collector as shown in Fig. 1d should not influence the thickness  
126 of the boundary layer. Since  $\delta_3 = \delta_4$ , flux measured in Fig 1d will represent the true  
127 length-averaged flux regardless of the length  $L_4$ . The value of  $v_t$  derived from disk 4 is  
128 the “true” value to be used for modeling indoor dynamics.

### 129 *1.3. Deviation of measured $v_t$ from “true” $v_t$*

130         Since the pollutant or surrogate species used for measuring  $v_t$  may not react  
131 rapidly with surfaces, a correction factor is necessary to generate the “true” value of  $v_t$ .  
132 The relative influence of the dimensions of the flux surface on the resulting value of  $v_t$

133 can be estimated by scrutinizing mass-transfer correlations for boundary layers in  
134 relevant aerodynamic systems (Table 1). For example, for developing flow (turbulent)  
135 over a planar surface the local value,  $v_t(x)$  is

$$136 \quad v_t(x) = 0.0296x^{-1} D Re_x^{4/5} Sc^{1/3} \quad (4)$$

137 where  $x$  is the distance along the surface from the upstream edge,  $Re_x$  is the Reynolds  
138 number ( $xu/\nu$ ),  $Sc$  is the Schmidt number ( $\nu/D$ ),  $u$  is the bulk velocity and  $\nu$  is the  
139 kinematic viscosity. Thus,  $v_t$  is proportional to  $x^{-0.2}$ . Each of the turbulent systems shown  
140 in Table 1 exhibits this weak dependence on dimension, suggesting that a size correction  
141 factor is small. This would be advantageous because the larger the correction factor, the  
142 larger the potential for error due to the correction. For example, for a measuring device  
143 dimension,  $L_t$ , of 0.15 m and a typical room dimension,  $L_c$ , of 2.5 m, the measured value  
144 of  $v_t$  will be roughly  $(0.15/2.5)^{-0.2}$  or 1.8 times greater than the “true” value. Although this  
145 may only apply to turbulent systems, measurements (Nazaroff et al., 1990) have indicated  
146 that indoor air movement can often be described as “homogeneously turbulent” and it  
147 may be reasonable to simply apply this correction factor based on the dimensions of the  
148 flux device and the room as suggested by (Morrison et al., 2003). Results derived from  
149 ozone deposition to coated filters, described in Methods, will be adjusted in this way by  
150 assuming homogeneous turbulence.

151 The generalized correction factor,  $f_L$ , for spatial differences is

$$152 \quad f_L = \frac{v_t(L_1)}{v_t(L_c)} = \left( \frac{L_1}{L_c} \right)^a \quad (5)$$

153 where the superscript  $a$  is equal to -0.2 for turbulent conditions. In contrast, for air flow  
154 that is not turbulent (Nazaroff and Cass, 1987), the appropriate correction may be

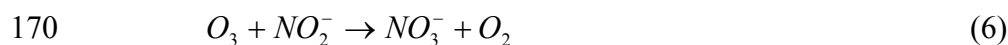
155 obtained from correlations appropriate to the existing fluid-mechanical conditions. From  
156 Table 1, it is apparent that  $a$  takes different values depending on the fluid-mechanical  
157 conditions and the system. Fig. 2 shows how the fraction,  $f_L$ , in Eq. (5) decreases as the  
158 ratio  $L_1/L_c$  decreases for laminar and turbulent duct flow. The error is minimized as the  
159 linear dimension of the measuring surface (see inset of Fig. 2) approaches the dimension  
160 of the room itself, assuming the correlations for duct flow can be extrapolated to indoor  
161 systems. A large absolute value of  $a$  is suggested for transition flow in a duct ( $a = -1.1$ )  
162 and laminar flow between parallel plates ( $a = -1.33$ ). The correction factor becomes  
163 exceedingly large for these systems.

164

## 165 **2. Methods**

### 166 *2.1 Analytical*

167 The local surface flux of ozone is quantified, using the DeVO method of (Morrison et al.,  
168 2003), by determining the rate at which nitrite ions on a prepared filter are converted to  
169 nitrate by the following reaction:



171 For each experiment, a coating solution of 100ml was prepared, including 1g of sodium  
172 nitrite, 1g of potassium carbonate, 0.2 g of erythritol (hygroscopic agent similar to  
173 glycerol) in a solvent of 70ml deionized water and 30ml of methanol. This solution was  
174 stored in a refrigerator at 4°C. Twelve glass fiber filters, 15 cm in diameter, were placed  
175 on horizontal nylon screens in an anaerobic glovebox. 5ml of the coating solution was  
176 applied onto each filter by 5ml pipette. The filters were then dried completely in the  
177 glovebox for 1 to 2 days and stored there until needed.

178 After an experimental exposure interval, discussed below, each sample filter was  
179 placed in a sealed plastic bag and ultrasonically extracted for 5 min with 100 ml  
180 deionized water. The extracts were filtered through 0.45  $\mu\text{m}$  nylon syringe filter and 5ml  
181 of the extract was injected into an ion chromatography system for analysis. The time-  
182 averaged mass transport-limited deposition velocity to the filter,  $\bar{v}_{t, \text{ozone}, \text{filter}}$ , is derived by  
183 assuming that a) the bulk ozone concentration is uniform throughout the room and b) the  
184 ozone concentration near the filter surface is almost zero due to low surface resistance to  
185 the overall mass transfer process. This transport limited behavior was verified by  
186 (Morrison et al., 2003).

$$187 \quad \bar{v}_{t, \text{ozone}, \text{filter}} = \frac{m_{\text{NO}_3} MW_{\text{O}_3}}{\bar{C}_{\text{O}_3} MW_{\text{NO}_3} A \Delta t} \quad (7)$$

188 where  $m_{\text{NO}_3}$  is the mass of nitrate formed on the filter (g),  $MW_{\text{O}_3}$  is the molecular weight  
189 of ozone ( $\text{g mol}^{-1}$ ),  $MW_{\text{NO}_3}$  is the molecular weight of the nitrate ion ( $\text{g mol}^{-1}$ ),  $\bar{C}_{\text{O}_3}$  is the  
190 time-averaged room concentration of ozone during the exposure interval ( $\mu\text{g m}^{-3}$ ),  $A$  is  
191 the exposed area of the filter ( $\text{m}^2$  or  $\text{cm}^2$ ) and  $\Delta t$  is the time interval exposed (h or s). The  
192 elapsed time,  $\Delta t$ , needed to quantify  $\bar{v}_{t, \text{ozone}, \text{filter}}$  depends on the lower detection limit of  
193 detection (LLD) of nitrate by IC, the purity of the nitrite salt, and the rate of ozone  
194 deposition. The LLD of  $\bar{v}_{t, \text{ozone}, \text{filter}}$  for the chamber experiment was  $0.05 \text{ cm s}^{-1}$  based on  
195 replicate chamber blank filters for which the standard deviation was  $3.6 \mu\text{g NO}_3^-$ .  
196 Therefore, the practical detection limit can be taken as  $36 \mu\text{g}$  per filter. This is equivalent  
197 to exposure of filters to 20 ppb ozone in the air for 5 hrs, 13 ppb in the air for 8 hrs with  
198  $\bar{v}_{t, \text{ozone}, \text{filter}} = 0.05 \text{ cm s}^{-1}$ .

199 Field measurements of  $\bar{v}_{t,ozone,filter}$  were converted to a “true” value of  $\bar{v}_{t,ozone}$  by  
200 assuming that fluid mechanical conditions reflected homogeneous turbulence. Using the  
201 correction factor defined by Eq (5),

$$202 \quad \bar{v}_{t,ozone} = \frac{\bar{v}_{t,ozone,filter}}{f_L} \quad (8)$$

203 where  $a = -0.2$  and  $L_c = 2.5$  m, using the room height as the characteristic length,  $L_c$ .  
204 These values are not corrected for systematic error associated with time-averaging  
205 (Morrison and Wiseman, 2005). Uncertainty in reported  $\bar{v}_{t,ozone}$  values is  $\pm 0.03$  cm s<sup>-1</sup>.

## 206 *2.2 Field Experiments*

207 *Laboratory and Office.* In a 10.1m × 7.4m laboratory, two DeVO filters, centers separated  
208 by 15 cm, were installed on a foam board false wall that was itself supported by an  
209 electronics rack at the location marked (\*) in Figure 3a. The sampling inlet of the ozone  
210 analyzer was located in the center of the lab. The two filters were exposed to air in this  
211 way for 12 h and the experiment was repeated three times over a period of five days. The  
212 spatial distribution of  $\bar{v}_{t,ozone}$  in this laboratory was evaluated in one experiment with nine  
213 more filters positioned at approximately equally spaced wall locations, also exposed for  
214 12 h. One set of measurements was performed in a laboratory space serving as an office  
215 for 10 graduate students. As in the laboratory experiment, two filters were placed near  
216 one another at a central location, \* in Fig 3b, and 9 other filters were distributed evenly  
217 around the perimeter of the room. The experiments were performed during the daytime to  
218 take advantage of higher natural ozone concentrations, which improved sensitivity of the  
219 DeVO method. The time interval,  $\Delta t$ , was 12 hrs.

220 *Apartment.* In an apartment (Figures 4a and 4b), two separate measurements of the spatial  
221 distribution of  $\bar{v}_{t, \text{ozone}}$  were obtained using nine DeVO filters spaced equally on walls in  
222 the living room and dining area. One additional filter was placed on the ceiling near a  
223 recirculation supply vent. To improve sensitivity, the window and door were kept open  
224 throughout the experimental period, increasing the average indoor concentration of  
225 ozone. Measurements were obtained with recirculation vents on (Fig 4a) and off (Fig 4b),  
226 respectively. The sampling inlet of ozone analyzer was located in the center of the living  
227 room.

### 228 *2.3 Influence of transport distribution on predicted mean flux*

229 Using the results of these experiments, an estimate is made of the range of error  
230 associated with using an area-averaged value,  $\hat{v}_t$ , instead of the true distribution to  
231 determine overall surface flux. Since the spatial distribution of ozone concentrations is  
232 not readily available, we assume that this distribution is similar to the spatial distribution  
233 of flux. For example, let  $\hat{v}_t = 0.2 \text{ cm s}^{-1}$  with a maximum of  $0.3 \text{ cm s}^{-1}$  and a minimum of  
234  $0.1 \text{ cm s}^{-1}$ . For this situation, we assume that for a volume-averaged ozone concentration  
235  $= 20 \mu\text{g m}^{-3}$ , the maximum local concentration at the edge of a concentration boundary  
236 layer will be  $30 \mu\text{g m}^{-3}$ , and the minimum will be  $10 \mu\text{g m}^{-3}$ . The range of error is  
237 determined using Eq. (2) and by allowing  $v_t$  and  $C_b$  to be correlated and anti-correlated.  
238 For the purposes of deriving the extremes of uncertainty, we assume that the ozone  
239 surface reaction probability,  $\gamma$ , equals 1, i.e. the surfaces are highly reactive.

### 240 **3. Results**

241 *Laboratory and Office.* Figures 3a and 3b show the spatial distribution of  $\bar{v}_{t, \text{ozone}}$   
242 measured in a working laboratory and an office area respectively. The diameter of the

243 circles is proportional to the transport-limited deposition velocity at the indicated  
244 locations. In the laboratory, the  $\bar{v}_{t,ozone}$  values near hoods, computers and on wide  
245 sidewalls or columns were greater than the  $\bar{v}_{t,ozone}$  values under cabinets, in corners and  
246 on central columns. This may be because mean air velocities are lower in the latter  
247 locations. Relatively consistent results were obtained at the position denoted by the  
248 asterisk, where three repeated measurements were obtained over the period of 5 days (see  
249 Figure 5).

250 Figure 3b shows the spatial distribution of  $\bar{v}_{t,ozone}$  measured in the occupied office  
251 space. The average of spatial measurements were not significantly different between the  
252 lab,  $0.14 \text{ cm s}^{-1}$ , or office,  $0.15 \text{ cm s}^{-1}$  nor were the standard deviations significantly  
253 different between the lab,  $0.04 \text{ cm s}^{-1}$ , or office,  $0.06 \text{ cm s}^{-1}$ .

254 *Apartment.* Figures 4a and 4b show the spatial distribution of  $\bar{v}_{t,ozone}$  in an  
255 apartment with the window and door open and the recirculation fans on (4a) and off (4b).  
256 With the recirculation fans on, the  $\bar{v}_{t,ozone}$  values at the location near the vent and window  
257 are very large due to high air velocities at these locations. The  $\bar{v}_{t,ozone}$  values at the  
258 location between two recirculation vents are much smaller and may be relatively stagnant  
259 locations. The average of measured values of  $\bar{v}_{t,ozone}$  is nearly double with the  
260 recirculation fan on,  $0.18 \text{ cm s}^{-1}$ , than with the fan off,  $0.10 \text{ cm s}^{-1}$ . The standard deviation  
261 for results with recirculation on,  $0.21 \text{ cm s}^{-1}$  is much greater than with the fan off,  $0.03$   
262  $\text{cm s}^{-1}$ . By excluding the near-vent filter measurement, the average and standard deviation  
263 of filters are nearly indistinguishable between fan-on and fan-off experiments. Although  
264 the average value of  $\bar{v}_{t,ozone}$  was higher with the recirculation fans on, some of the filter

265 locations experienced lower individual mass-transfer rates. Figure 5 demonstrates that co-  
266 located measurements (separated by 15 cm) result in flux that is within 20% of one  
267 another, whereas the range of values measured in other locations throughout the room is  
268 much greater. Most of the results from the laboratory studies and from the apartment are  
269 within the expected range of values of  $\bar{v}_{t,ozone}$  (Nazaroff et al., 1993).

270 *Distribution and the influence on predicted indoor concentrations.*

271 Using the  $\bar{v}_{t,ozone}$  spatial distribution as a guide, we generated a series of possible  
272 flux distributions for hypothetical rooms. Beginning with the apartment (no recirculation)  
273 results, and assuming that the outer boundary layer ozone concentration is spatially  
274 uniform, the estimated area-averaged flux is  $0.0193 \mu\text{g m}^{-2}$ . If the boundary layer ozone  
275 concentration distribution positively correlates with  $\bar{v}_{t,ozone}$ , the predicted area-averaged  
276 flux is  $0.0186 \mu\text{g m}^{-2}$ . If the outer boundary layer ozone concentration distribution  
277 inversely-correlates with  $\bar{v}_{t,ozone}$ , the predicted area-averaged flux is  $0.0173 \mu\text{g m}^{-2}$ .

278 Therefore, we observe a deviation of 4 to 11% compared with a uniform distribution  
279 assumption. Applying the same operation on the apartment results (with recirculation),  
280 the estimated deviation is 45 to 57%. Analyzing flux distributions in the laboratory and  
281 office, we find deviations ranging from 6 to 14%. In all cases, allowing the boundary  
282 layer concentration distribution to correlate with  $v_t$ , results in area-averaged flux that is  
283 lower than allowing the boundary layer concentration of ozone to be spatially uniform.

## 284 **4. Discussion**

### 285 *4.1 Spatial distribution of flux*

286 The laboratory, office and apartment results demonstrate that there can be a wide  
287 distribution of surface flux in a single room. As anticipated, areas near vents and other

288 sources of air movement tend to exhibit higher relative values of  $\bar{v}_{t,ozone}$ . Both  
289 measurements near operating computers (0.19 and 0.22 cm s<sup>-1</sup>) were roughly twice the  
290 value measured under cabinets or at most desks (0.09 – 0.14 cm s<sup>-1</sup>). The flux near the  
291 apartment recirculation register is demonstrated to be nearly 7 times greater than the  
292 average of all other spatial measurements in the apartment. Yet, excluding this  
293 measurement, the distribution of fluxes appear similar between the two apartment  
294 experiments. Flux on walls in unobstructed areas in the laboratory appears to be higher  
295 than in other locations; this effect was not observed in the apartment.

296         Filters located within ~ 1 meter of one another are observed to measure roughly  
297 the same flux, even in repeated measurements over 5 days. This finding suggests that  
298 there exists a limited number of measurement locations required to evaluate the  
299 distribution in a room. For example, an uninterrupted expanse of wall may require only a  
300 few measurements, and only a few “under-cabinet” measurements may be needed.  
301 Complicated geometry or locations near registers and windows likely require a higher  
302 density of measurements.

303         It is important to recall that a key, and most likely erroneous, assumption in the  
304 determination of local  $\bar{v}_{t,ozone}$  is that the bulk concentration is uniform. If not, then these  
305 values of  $\bar{v}_{t,ozone}$  only reflect the relative flux to those locations, not the true values of  
306  $\bar{v}_{t,ozone}$ . Mass-transfer coefficient measurement methods that employ the evaporation of a  
307 pure substance side-step the bulk concentration distribution problem because  $C_b$  can be  
308 ignored in Eq. (2) as being insignificant compared to  $C_s$ .

309         This uncertainty in the spatial distribution of concentration and transport intensity  
310 will also limit certainty in quantifying surface flux that is used in exposure models. A

311 good method of determining the surface source/sink term of these models is to measure  
312 inlet and outlet pollutant concentrations of a building while accounting for all other  
313 sources and sinks (Weschler et al., 1989). The area-averaged flux derived from this  
314 method is accurate for that building at that time, but internal transport or concentration  
315 distributions are not constant. Using our measured flux distribution as a guide, we can see  
316 that indoor surface flux predictions may be in error by up to 50% for highly surface-  
317 reactive species. If surfaces are the primary pollutant sink, then exposure estimates can be  
318 fairly uncertain. In the case of ozone, the surface reaction probability is moderate,  
319 meaning that the uncertainty in the surface-sink term, and exposure, will generally be  
320 smaller or perhaps negligible.

#### 321 *4.2 Recommendations for field measurements*

322       Having established that a distinct spatial variation in flux to indoor surfaces  
323 exists, how should future measurements be performed? There are several key issues that  
324 must be addressed before collecting indoor flux data. The analyses from sections 1.2 and  
325 1.3 demonstrate that the development of a concentration boundary layer over the  
326 measuring surface depends on the species measured. If a depositing species reacts  
327 completely with other indoor surfaces, then the “natural” boundary layer will not be  
328 disturbed and consideration of the fluid-mechanical state is unnecessary. Otherwise, some  
329 method of determining the fluid-mechanical state may need to be employed. In either  
330 case, the spatial distribution of concentration must be considered. Finally, an evaluation  
331 of temporal influences on flux (Morrison and Wiseman, 2005) suggests that a semi-  
332 instantaneous measure of surface flux may be necessary to avoid bias resulting from  
333 time-varying transport conditions. In lieu of an ideal, well-instrumented method, a

334 combination of techniques would likely provide sufficient information about spatial and  
335 temporal distributions and simultaneously provide for error correction. In general, at least  
336 one continuous/instantaneous measure of conditions, such as microbalance flux or air  
337 velocity (Morrison et al., 2003), and two sizes of deposition/emission flux surfaces  
338 maybe employed simultaneously. Combined, these methods allow the researcher to de-  
339 convolute errors imposed by the independent limitations of each device. With these as  
340 considerations in mind, we discuss four different scenarios for determining the transport  
341 limited deposition velocity of various species.

#### 342 4.2.1 Deposition of ozone and spatial distribution of $\bar{v}_{t,ozone}$ .

343 In this example, we consider mass-transfer analyses in a room (see Fig. 2 inset)  
344 that is similar to the methods employed for the spatial distribution shown in Figs. 3 and 4.  
345 Distributed around the room are several small filters ( $L_1$ ) coated with  $\text{NaNO}_2$  for  
346 determining a time-averaged flux of ozone at those locations. In addition several larger  
347  $\text{NaNO}_2$  filters ( $L_2$ ) are located near, but not immediately adjacent to, the smaller filters.  
348 The gas-phase concentration of ozone is measured continuously using a photometric  
349 ozone analyzer in the center of the room. Using Eq. (7) a location specific  $\bar{v}_{t,ozone}$  for each  
350 filter is obtained after 8 hours. A micro-balance based evaporative flux instrument  
351 providing an instantaneous, local result is deployed on one wall (cross-hatched circle).  
352 This evaporative method, a.k.a. DeVS, is described in detail in Morrison et al. (2003).  
353 Briefly, octadecane evaporates from a quartz-crystal microbalance and the flux is  
354 converted into an instantaneous mass-transfer coefficient using Eq. 1. Error correction  
355 can now be applied in a two step fashion:

356 1) Because the flow characteristics are unknown, the coefficient  $a$  in Eq. (5) is unknown.  
357 Instead, results from the small ( $L_1$ ) and large ( $L_2$ ) filters are combined to estimate the  
358 value of  $a$  by rearranging Eq. (5), and replacing  $L_c$  with  $L_2$ :

$$359 \quad a = \ln \left( \frac{\bar{v}_{t,L_1}}{\bar{v}_{t,L_2}} - \frac{L_1}{L_2} \right) \quad (9)$$

360 This is used to correct, at each location, for the error which is due to the limited size of  
361 the filters used to determine ozone flux. For each location, Eq. (5) is solved for  $f_L$ , using  
362 the characteristic dimension, e.g. height, of the room,  $L_c$ .

363 It should be noted that determination of  $a$  inherently corrects for uncertainty in the  
364 relative reactivity of the surface, parameterized by the surface reaction probability,  $\gamma$ . For  
365 species with a low surface reaction probability, e.g. a solvent,  $a$  is the maximum value  
366 associated with the fluid mechanical conditions. For species with a high surface reaction  
367 probability, e.g. nitric acid,  $a$  should be near zero. Species of moderate surface reactivity,  
368 e.g. ozone, the value of  $a$  will fall somewhere in-between the high and low reactivity  
369 cases.

370 Error due to time-averaging can now be corrected by using the continuous  $v_t$   
371 measurement. A value for the correction factor,  $f_t$  is obtained from Eq. (16) of (Morrison  
372 and Wiseman, 2005). The corrected value at location 1 is now,

$$373 \quad \bar{v}_{t,1,corrected} = \frac{\bar{v}_{t,L_1}}{f_t f_L} \quad (10)$$

374 The absolute value at the continuous measurement location must also be corrected for its  
375 small dimensions:

$$376 \quad v_{t,corrected}(t) = \frac{v_t(t)}{f_L} \quad (11)$$

377 Note that no spatial measurement of ozone concentrations was recommended. It is  
378 unclear how to make this field measurement in practice without disturbing the system  
379 with a forest of sample tubing. Spectroscopic methods (Drescher et al., 1996) may not be  
380 sensitive enough to resolve ozone spatially at typical ppb indoor mixing ratios.

381 4.2.2 Deposition of nitric acid and spatial distribution of  $\bar{v}_{t,HNO_3}$ .

382 In this example, distributed filters are used to collect nitric acid, a species that is  
383 expected to deposit irreversibly with all indoor surfaces. With such a high reaction  
384 probability, the act of collecting nitric acid does not influence the existing concentration  
385 boundary layer and consideration of fluid-mechanical conditions is unnecessary.  
386 Therefore, the size of the collecting surface is unimportant. Yet, a continuous  
387 measurement afforded by the DeVS device is still required. Morrison and Wiseman  
388 (2005) show that for depositing species with high reaction probabilities, bias associated  
389 with time-varying conditions is maximized.

390 4.2.3 Deposition of carbon dioxide used to determine spatial distribution of  $\bar{v}_{t,ozone}$

391 As explained in Morrison and Wiseman (2005), it is not necessary to use ozone  
392 itself to determine  $\bar{v}_{t,ozone}$ . Instead a surrogate species can be used in combination with a  
393 correction factor to determine the mass-transfer coefficient of a target species. In this  
394 example, filters coated with LiOH are used to collect carbon dioxide by the reaction



396 Titration of the extracted filters provide information used to determine flux and  $\bar{v}_{t,CO_2}$ .  
397 Because CO<sub>2</sub> does not deposit to any substantial degree on indoor surfaces, i.e. a low  
398 surface reaction probability, two sizes of filters are again used (as in 4.2.1) to correct for

399 boundary layers of uncertain thickness that develop over the filters. Using Eq. 15 of  
400 Morrison and Wiseman (2005),  $\bar{v}_{t,ozone}$  can be evaluated at each filter location

$$401 \quad \bar{v}_{t,ozone} = \bar{v}_{t,CO_2} \left( \frac{D_{CO_2}}{D_{ozone}} \right)^{0.67} \quad (13)$$

402 where  $D$  is the diffusion coefficient of the subscripted compound. The analysis of  
403 (Morrison and Wiseman, 2005) suggests that time-varying conditions may bias results  
404 even for some surface unreactive compounds such as  $CO_2$ . Therefore, the DeVS device is  
405 deployed in this example as well. Since  $CO_2$  mixing ratios are generally in the  $>500$  ppm  
406 range, a spatial measurement (Drescher et al., 1996) may be possible, but cumbersome.

407 4.2.3 Emission of octadecane used to determine spatial distribution of  $\bar{v}_{t,ozone}$

408 In this example, we suggest employing a surrogate species, once again, to  
409 determine  $\bar{v}_{t,ozone}$ . However, the emission of an evaporating hydrocarbon from a surface is  
410 employed instead of deposition, since both processes are mirror images under the same  
411 fluid-mechanical conditions. To enhance our understanding of both spatial and temporal  
412 distributions within a room, we employ a suite of microbalance based DeVS devices  
413 coated with octadecane (Morrison et al., 2003). To account for uncertainty in fluid-  
414 mechanical conditions, half of the DeVS devices are coated with octadecane to a  
415 diameter of 15 cm; the rest of the units are coated to a diameter of 30 cm. These values  
416 are arbitrary, and just used to illustrate the system. This is effectively the same as using  
417 two different filter sizes as suggested in 4.2.1 and 4.2.3. There is no need to measure the  
418 spatial distribution of gas-phase octadecane concentrations because the evaporation rate  
419 is so small that the outer boundary layer concentration is effectively zero and near surface  
420 concentration depends only on the temperature of the coating.

421 Will these corrected methods provide robust values needed for indoor air quality  
422 modeling and exposure assessment? Until the experimental evidence is in hand, these  
423 recommendations are tentative. The fact that it is impossible to co-locate  
424 collecting/emitting surfaces makes the corrections, Eqs. (10) and (11), somewhat  
425 uncertain but better than no correction, since our results show that a 20% uncertainty in  
426 co-located DeVO filters is to be expected.

## 427 **8. Conclusions**

428 The measurement accuracy of heat and mass-transfer coefficients in practice is  
429 limited. By measuring spatial distributions in indoor settings, we demonstrate that fluxes  
430 vary widely with location. Spatial gradients in concentration and flux make simple  
431 exposure analysis less certain. Error associated with the use of devices of dimensions  
432 smaller than the size of the room is more severe than that due to uncertainty in the spatial  
433 concentration of the depositing species. Researchers tempted to map out the spatial  
434 distribution of mass-transfer coefficients with small filters or other devices may observe  
435 much larger mass-transfer coefficients than the “true” values. Before initiating a study of  
436 this sort, the device size, room-surface reaction probability of the species collected, and  
437 flow conditions must all be considered so that a reasonable estimate of the mass-transfer  
438 coefficient can be obtained with thoughtful error correction. The two-step procedure for  
439 error correction recommended here should generate a best-estimate of the local mass-  
440 transfer coefficient.

441

## 442 **Acknowledgements**

443

444 This material is based upon work supported by the National Science Foundation under  
445 Grant No. 0238721. Priscilla Morrison for significantly improving the manuscript and the  
446 folks from the UMR pre-tenure writer's group for their helpful suggestions.

447

448 **References**

449 Drescher, A. C., Gadgil, A. J., Price, P. N., Nazaroff, W. W. 1996. Novel approach for  
450 tomographic reconstruction of gas concentration distributions in air: Use of smooth basis  
451 functions and simulated annealing. *Atmospheric Environment* 30(6): 929-940.

452

453 Morrison, G. C., Wiseman, D. J. 2005. Temporal considerations in the measurement of  
454 indoor mass-transfer coefficients. *Atmospheric Environment* in submission.

455

456 Morrison, G. C., Zhao, P., Wiseman, D. J., Ongwande, M., Chang, H., Portman, J.,  
457 Regmi, S. 2003. Rapid measurement of indoor mass-transfer coefficients. *Atmospheric*  
458 *Environment* 37: 5611-5619.

459

460 Nazaroff, W. W., Cass, G. 1987. Particle deposition from a natural convection flow onto  
461 a vertical isothermal flat plate. *Journal of Aerosol Science* 18(4): 445-455.

462

463 Nazaroff, W. W., Gadgil, A. J., Weschler, C. J. 1993. Critique of the use of deposition  
464 velocity in modeling indoor air quality. *Modeling of indoor air quality and exposure*. N.  
465 L. Nagda. Philadelphia, PA, American Society for Testing and Materials. ASTM STP  
466 1205: 81-104.

467

468 Nazaroff, W. W., Ligocki, M. P., Ma, T., Cass, G. 1990. Particle deposition in museums:  
469 Comparison of modeling and measurement results. *Aerosol Science and Technology*  
470 13(3): 332-348.

471

472 Shah, R. K., Bhatti, M. S. 1987. *Handbook of single-phase convective heat transfer*. New  
473 York, Wiley-Interscience.

474

475 Weschler, C. J., Shields, H., Naik, D. V. 1989. Indoor ozone exposures. *JAPCA: Journal*  
476 *of the Air and Waste Management Association* 39: 1562-1568.

477

478 **Figure and Table Captions**

479

480 **Fig. 1.** Concentration boundary layer development over indoor surfaces with and without  
481 measurement devices: (a) collecting/emitting device of length  $L_1$  develops a boundary  
482 layer with a center thickness  $\delta_1$ ; (b) collecting/emitting device of length  $L_2$  develops a  
483 boundary layer with a center thickness  $\delta_2$ ; (c) boundary layer over walls (at corner) for a  
484 highly surface reactive species such as a gas-phase acid; (d) boundary layer over walls (at  
485 corner) for a highly surface reactive species, including collecting surface with length  $L_4$ .

486 **Fig. 2.** The ratio,  $f_L$ , for turbulent and laminar duct flow vs the ratio  $L_1/L_2$ . Inset: room  
487 outfitted with two different sizes of time-averaged flux measurement disks  $\otimes$ , a  
488 continuous flux measuring device  $\oplus$ , and a gas-measurement method.

489 **Fig 3.** Spatial distribution of  $v_{t,ozone}$  in (a) a working laboratory and (b) a laboratory room  
490 used as student offices. The diameter of the circle corresponds to the intensity of ozone  
491 flux at that location.

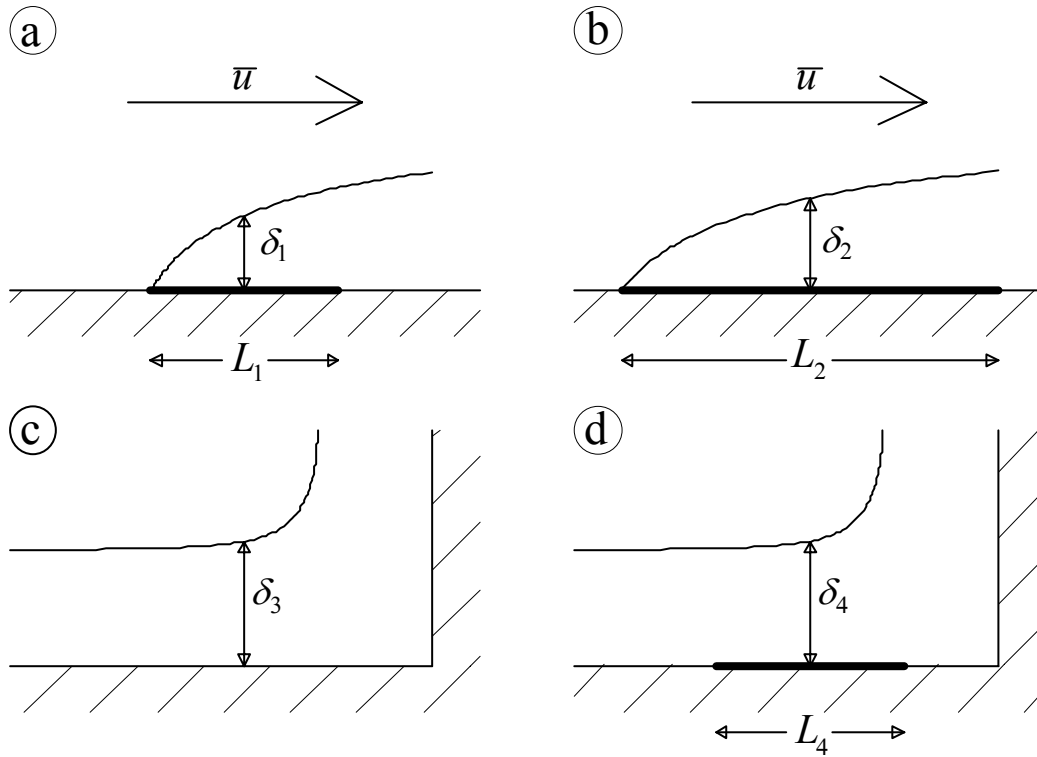
492 **Fig 4.** Spatial distribution of  $\bar{v}_{t,ozone}$  in an apartment with (a) the recirculation fan on and  
493 (b) the recirculation fan off. The diameter of the circle corresponds to the intensity of  
494 ozone flux at that location.

495 **Fig 5.** Co-located measurements of  $\bar{v}_{t,ozone}$  on a central column in a working laboratory  
496 over a 10 day period and distribution of  $\bar{v}_{t,ozone}$  throughout a room on a single day.

497

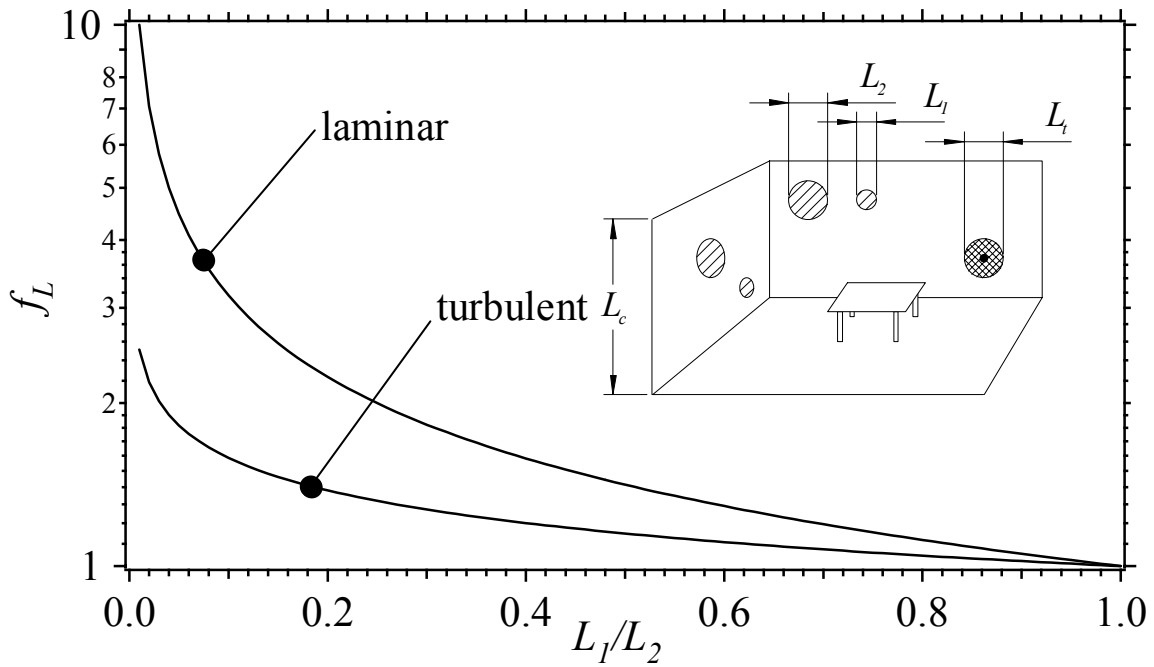
498 **Table 1.** Mass-transfer correlations for various configurations and flow conditions.

499 **Figure 1**



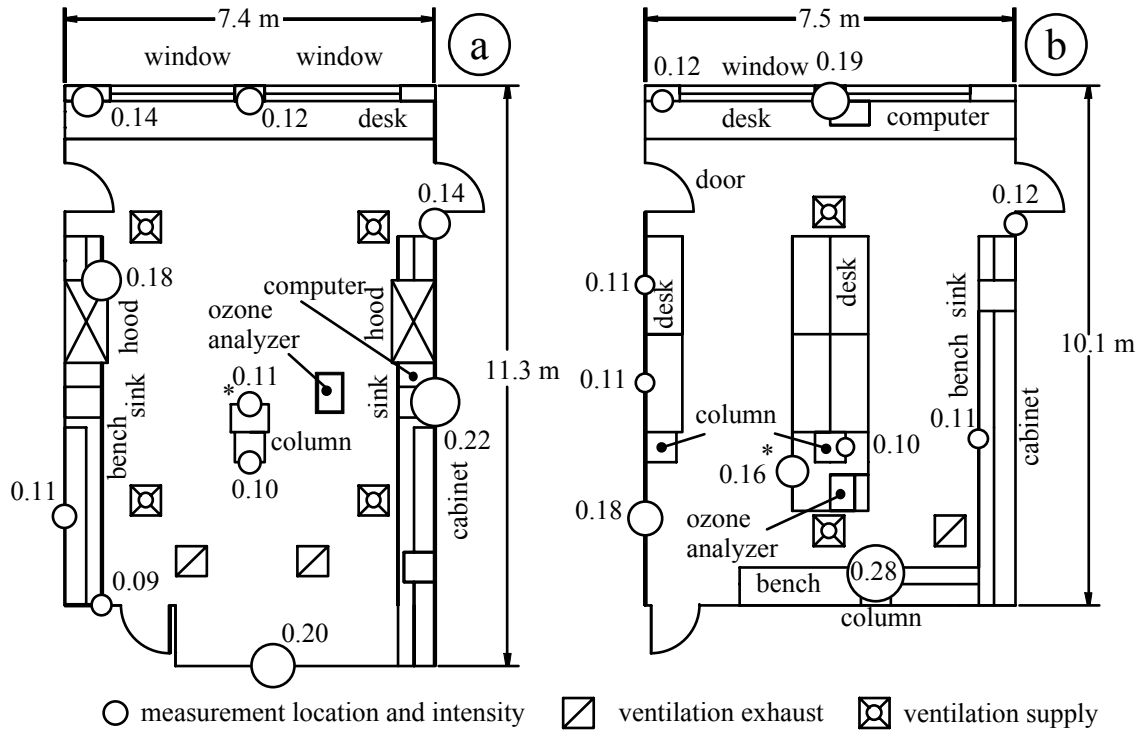
500

501 **Figure 2**



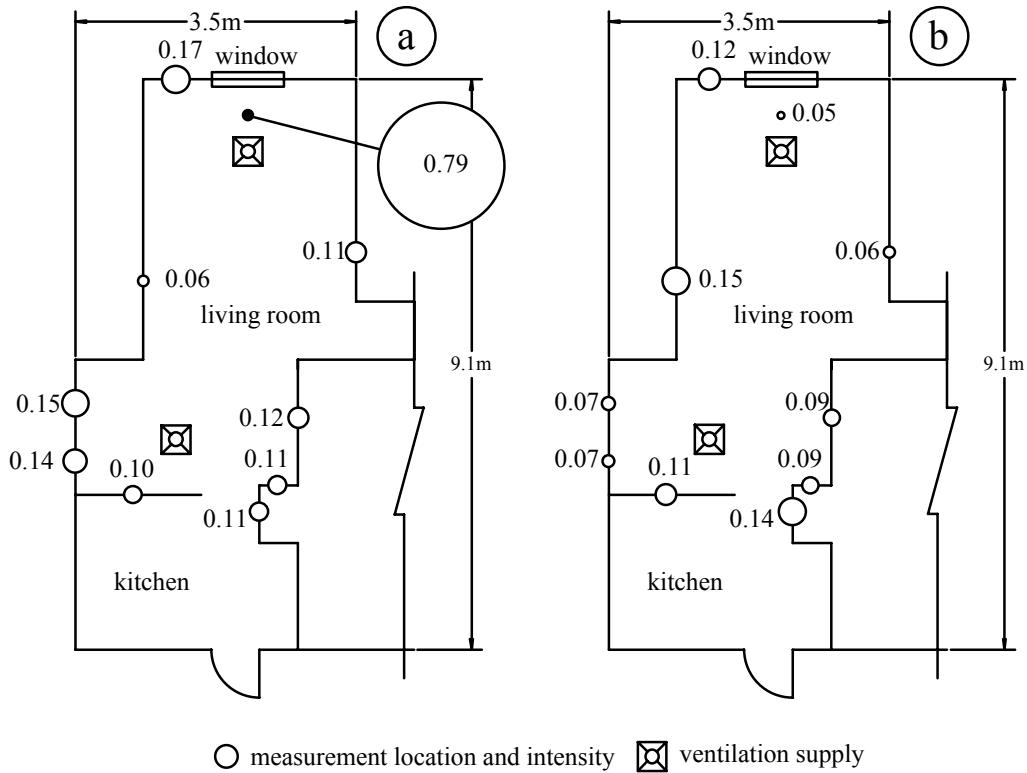
502

503 Figure 3



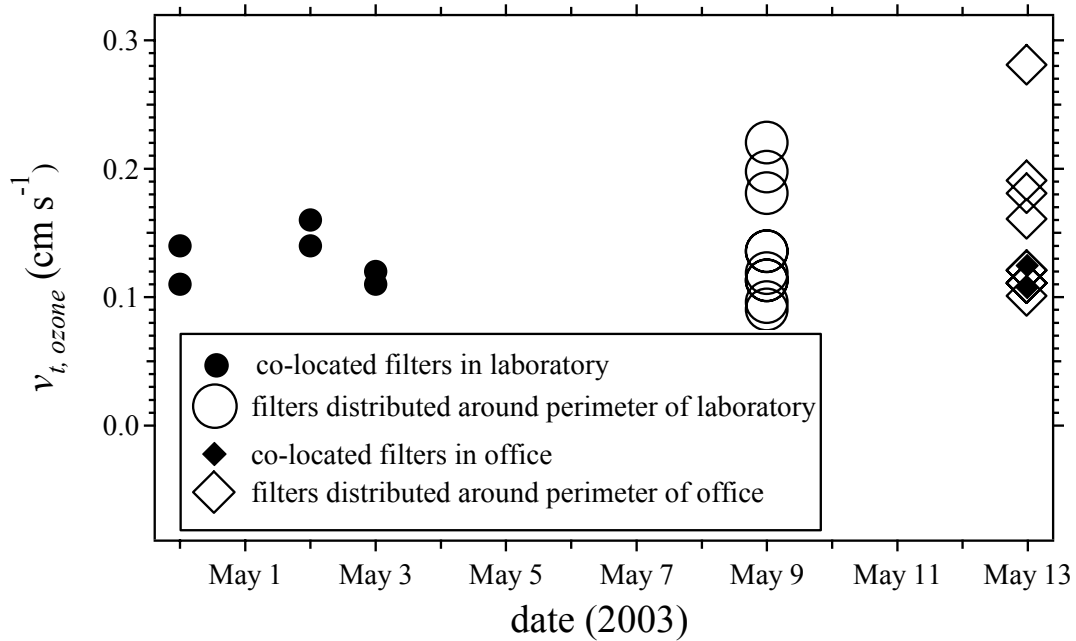
504

505 Figure 4



506

507 Figure 5



508

509 **Table 1**

System	fluid mechanical region	Local $v_{t,x} =$	Length average $v_{t,L} =$	$\frac{v_t(L_1)}{v_t(L_2)} = \left(\frac{L_1}{L_2}\right)^n$ $n =$
Duct	Laminar	Eq. 3.48-3.49 Kakaç†		-(1.1 to 1.7)
	transition	Eq. 4.31-4.35 Kakaç†		-1.1
	turbulent	$0.023x^{-1} D Re_x^{0.8} Sc^{1/3}$		-0.2
Planar surface	laminar	$0.332x^{-1} D Re_x^{1/2} Sc^{1/3}$	$0.664L^{-1} D Re_L^{1/2} Sc^{1/3}$	-0.5
	turbulent	$0.0296x^{-1} D Re_x^{4/5} Sc^{1/3}$	$0.02376L^{-1} D Re_L^{4/5} Sc^{1/3}$	-0.2
Parallel plates	laminar	$\frac{2xD Re_{Dh}^{1/3} Sc^{1/3}}{\Gamma(4/3)\left(\frac{6x}{D_h}\right)^{1/3}}$	$\frac{4xD Re_{Dh}^{1/3} Sc^{1/3}}{3\Gamma(4/3)\left(\frac{6x}{D_h}\right)^{1/3}}$	-1.33
	transition	$0.116(Re^{.666} - 160)Sc^{1/3} \left[ 1 + \left(\frac{x}{D_h}\right)^{-.666} \right]$		-0.67
	turbulent	Eq. 4.104 Kakaç†	Eq. 4.105-4.106 Kakaç†	-(0.16 to 0.26)
Notes: Reynolds number, $Re_{L,x}=uL/\nu$ , where $u$ is the net fluid velocity, $L$ is the characteristic length (e.g. height of room or length of flux surface) or $x$ is the distance along the surface, $\nu$ is the kinematic viscosity. $D_h$ is the hydraulic diameter of the system, duct or parallel plates. Schmidt number, $Sc = \nu/D$ , where $D$ is the diffusion coefficient of the transporting species Correlations all derived from (Shah and Bhatti, 1987) †For brevity these equations are not shown in this table but are found in Shah and Bhatti (Shah and Bhatti, 1987)				

510